CHEMISTRY
A European Journal

A Journal of
ChemPubSoc Europe

Accepted Article

Title: Exploring the Phase-Selective, Green Hydrothermal Synthesis of Upconverting Doped Sodium Yttrium Fluoride: Effects of Temperature, Time and Precursors

Authors: Nora Jannsen, Stefano Diodati, Nicola Dengo, Francesca Tajoli, Nicola Vicentini, Giacomo Lucchini, Adolfo Speghini, Denis Badocco, Paolo Pastore, and Silvia Gross

To be cited as: *Chem. Eur. J.* 10.1002/chem.201903261

Link to VoR: http://dx.doi.org/10.1002/chem.201903261

Supported by
ACES

WILEY-VCH

10.1002/chem.201903261

FULL PAPER

Exploring the Phase-Selective, Green Hydrothermal Synthesis of Upconverting Doped Sodium Yttrium Fluoride: Effects of Temperature, Time and Precursors

Nora Jannsen,[a,b] Stefano Diodati,[a,c] Nicola Dengo,[a,c] Francesca Tajoli,[a,c] Nicola Vicentini,[a,c] Giacomo Lucchini,[d] Adolfo Speghini,[d] Denis Badocco,[a] Paolo Pastore[a] and Silvia Gross*[a,c]

Abstract: The aim of this work was i) to develop a hydrothermal, low temperature synthesis protocol affording the upconverting hexagonal phase $NaYF_4$ with suitable dopants while adhering to the õgreen chemistryò standards and ii) to explore the effect that different parameters have on the products. In optimizing the synthesis protocol, short reaction times and low temperatures (below 150 °C) were considered. Yb^{3+} and Er^{3+} ions were chosen as dopants for the $NaYF_4$ material. Within the context of the second goal, parameters including nature of the precursors, treatment temperature and treatment time were investigated in order to afford a pure hexagonal crystalline phase, both in the doped and undoped materials. To fully explore the synthesis results, the prepared materials were characterized from a structural (XRD), compositional (XPS, ICP-MS) and morphological (SEM) point of view. The upconverting properties of the compounds were confirmed by photoluminescence measurements.

Introduction

In the last decades, numerous investigations have been carried out on upconverting materials.[1] Upconversion (UC) is a process which can be considered an anti-Stokes emission with respect to the exciting radiation and represents a simple and effective opportunity for many technological applications, for instance in photonics, optical codification and sensing applications.[2]
The UC process opens up application possibilities in several optical recognition systems, for example those used in anti-counterfeit labels.[3] To make these systems accessible to large scale applications, it is important to develop cheap and facile synthesis routes for the desired materials.
$NaYF_4$, one of the most efficient upconverters, can crystallize as two polymorphs. The cubic Ŭ-phase (space group $Fm\bar{3}m$), also known as the high temperature modification, can be described as a fluoride structure, in which the cation sites are randomly occupied by sodium and yttrium. In this structure, the cations build a cubic close packed structure and the fluoride anions occupy each tetrahedral gap. The cations are surrounded cubically by fluorides with a coordination number of eight, whereas each fluoride ion is tetrahedrally coordinated.[4] On the other hand, the hexagonal ƀ-$NaYF_4$ ($P\bar{6}$ space group)[5] crystallizes into a phase that is a variant of the gagarinite structure.[4] It is this latter phase that was the focus of our attention for the preparation of upconverting materials.
When suitably doped with rare earth (RE) elements, such as Yb^{3+} and Er^{3+} ions, sodium yttrium fluoride is capable of upconversion, mainly exploiting the $Yb^{3+} \rightarrow Er^{3+}$ energy transfer. Energy Transfer Upconversion (ETU) occurs among Yb^{3+} and Er^{3+} ions, that have similar energy levels. Moreover, a fluoride-based host is endowed by a low phonon energy, whereby the multiphonon relaxation channel can remain small, improving emission efficiency and lengthening the lifetimes of the excited energy levels. Because of the relatively long lifetimes of these metastable levels (up to some milliseconds), the sensitization by ETU is much more effective in the case of this system compared to other upconversion mechanisms like Excited State Absorption (ESA).[2a, 2b]
The two doping ions have different roles regarding the upconverting mechanism: while ytterbium has the role of sensitizer, erbium acts as an activator. If near infrared (NIR) light with a wavelength of 980 nm irradiates the upconverting particles, electrons in the ytterbium ion $^2F_{7/2}$ ground state are excited into the higher-level state $^2F_{5/2}$. This step is followed by the sensitization of the activator Er^{3+} in two successive steps. First electrons are promoted from the ground state $^4I_{15/2}$ into the metastable state $^4I_{11/2}$. Due to its long life-time, a high occupation of this level is possible and a second excitation can follow, including the occupation of $^4F_{7/2}$. Green emission occurs from the $^2H_{11/2}$ and $^4S_{3/2}$ levels with wavelengths of 521 nm and 543 nm respectively. [2a, 2b]

[a] Prof. S. Gross, N. Jannsen, Dr. S. Diodati, N. Dengo, F. Tajoli, Dr. Vicentini, Prof. D. Badocco, Prof. P. Pastore
Dipartimento di Scienze Chimiche
Università degli Studi di Padova
Via Marzolo 1, 35131 Padova, Italy
Email: silvia.gross@unipd.it
[b] Nora Jannsen
Institute of Inorganic and Applied Chemistry
University of Hamburg
20146 Hamburg, Germany
[c] Prof. S. Gross, Dr. S. Diodati, N. Dengo, F. Tajoli, Dr. Vicentini
INSTM, UdR di Padova
Via Marzolo 1, 35131 Padova, Italy
[d] Dr. G. Lucchini, Prof. A. Speghini
NRG, Dipartimento of Biotecnologie
Università di Verona and INSTM, RU Verona
Strada Le Grazie 15, I-37314 Verona, Italy

Supporting information for this article is given via a link at the end of the document.

10.1002/chem.201903261

Additional relaxation steps lead to the occupation of $^{4}F_{9/2}$ and, ultimately, to the emission of red light with a wavelength of 657 nm.

For application purposes, it is important to develop a synthetic approach that allows the formation of materials characterized by uniform properties throughout the sample and high crystallinity. Monodispersed particles can be obtained by hydrothermal synthesis, which is defined as a heterogeneous reaction in aqueous solvent at high temperatures (above the 100 °C) and a pressure over 1.[6] Those conditions can be easily reached by using a heated pressure resistant closed vessel (autoclave), where the pressure increases simply as a consequence of vapor confinement upon heating (autogenous pressure). As a result of the nonstandard conditions thus achieved, physical properties, such as viscosity, ionic product and dielectric constant undergo changes. This affects the solubility, as well as nucleation and growth behavior, of the involved species and enables syntheses which are inconceivable in normal conditions. Water, for example, becomes a much more nonpolar solvent, allowing the solubilization of normally insoluble reactants and the crystallization of new products.[6b, 7]

Despite the facile protocols, a narrow size distribution and a large variety of sizes, shapes and crystalline phases can be reached. For hexagonal $NaYF_4$, crystals, prisms, disks, tubes, rods and octahedral shapes were obtained, depending on the reaction conditions, such as the fluoride source, the pH and organic additives.[8]

As an example, Wang *et al*. carried out several hydrothermal syntheses at 240 °C changing the molar ratio between the reactants (NaF and lanthanide oxides), yet were able to obtain cubic nanoparticles, mixtures of cubic and hexagonal nanoparticles and hexagonal nanorods for F/Ln ratios of 5, 10 and 12 respectively.[9]

Further investigations concerning the role of the solvent evidenced that, in syntheses with equal reactant molar ratios, water as a solvent led to cubic phases, whereas ethanol (and therefore implying a switch to solvothermal synthesis) to hexagonal ones.[9]

In general, reports found in the literature for the hydrothermal synthesis of sodium yttrium fluoride always required temperatures of 180 °C or above[10] and/or additives such as polyethylene glycol or imines.[8] To the best of our knowledge, this is the first time a synthetic approach is reported upon whereby $NaYF_4$ is obtained at 150 °C in surfactant-free conditions.

Apart from hydrothermal synthesis, the thermal decomposition is another common approach employed to synthesize doped $NaYF_4$: such syntheses are usually performed with rare earth trifluoroacetate precursors in noncoordinating and high boiling solvents such as octadecene or oleylamine. The precursors decompose at relatively low temperatures (between 200 and 300 °C) to the corresponding fluoride.[11]

Given the interest in gaining a good control over the characteristics of the prepared materials, as well as the importance in understanding how the synthetic process proceeds, it is important to gain insight on the effect that a change in the synthesis parameters will have on the resulting products. It is furthermore important to try to achieve easy and low temperature protocols affording good tunability for the final materials whilst following the principles of ñgreen chemistryò. In particular, the optimized synthetic approach is compliant with three of the 12 ñGreen Chemistryò principles (3, 5 and 6),[12] as it pursues less hazardous chemical syntheses, is based on safer solvents (i.e. water) and does not require further auxiliaries or demanding work-up of the products. Concerning paradigm 6 (Design for energy efficiency), the optimized hydrothermal treatment features, due to the low temperature involved, a relatively low energy consumption.

Within this dual scope, a low-temperature hydrothermal synthesis protocol was optimized for doped upconverting hexagonal sodium yttrium fluoride. Numerous synthetic runs were carried out to investigate the effect of synthesis time, temperature, nature and nominal ratio of the precursors on the structural, compositional and functional characteristics of the resulting materials. The investigation of the parameters explored in this study represents a systematic optimization work over a large number of synthetic experiments (over 40 samples) the purpose of which was to determine the optimal parameters set for the synthesis of upconverting particles, as well as, indirectly, to see if such parameters could be adjusted to achieve a more efficient synthesis, as well as better performing products as far as luminescence properties are concerned. Indeed, the main reason why synthetic runs exploring lower temperatures and shorter treatment times were carried out, was to see how these parameters influenced the products and therefore what the minimum requirements were for the desired phase to be obtained. The protocol was accordingly optimized with the aim of shortening reaction times and lowering temperatures. An interesting effect of selected experimental parameters and phase-selection pursuit was pointed out.

Results and Discussion

Synthesis of undoped $NaYF_4$

Effect of precursors

In order to achieve the target of optimizing an efficient and simple low-temperature route for preparing an effective and high-performing upconverting material, an initial stage of the work was focused on the synthesis of undoped $NaYF_4$. This preliminary investigation served to the purpose of yielding information on the lattice which would then serve as the host in the lanthanide doped fluorides.

It was initially important to figure out what the ideal parameters were to synthesize the host lattice in the desired crystalline form, in the case of sodium yttrium tetrafluoride particles the hexagonal phase (ϐ-$NaYF_4$). Regarding the atomic ratio of the elements in the chemical formula, this reaction was assumed to occur:

ὣ ΰΰ, , ﻂ τΰὣ΄0 ɫ ΰὣὣ΄ʠ ﻂ σΰὣΰΰ, (Eq. 1)

For this reason, a 48-hour reaction with an yttrium to sodium atomic ratio of 1:4 was initially attempted (see Table 9 in the Experimental Section). The observed behavior differed from expectations: XRD analyses (Figure 1) evidenced that a mixture of cubic (as opposed to hexagonal) $NaYF_4$ and YF_3 resulted. By decreasing the ratio of sodium fluoride over to yttrium nitrate (to

10.1002/chem.201903261

FULL PAPER

2:1), no product except YF_3 could be achieved. This result agrees with the reported sodium fluoride-yttrium fluoride phase diagram,[13] which reveals the formation of orthogonal yttrium fluoride at molar percentages above 52 % (with regard to YF_3). With higher Y/F molar ratios, the results improved; additionally, YF_3 was not formed if the Y/F molar ratio was 1:6 or higher. If eight equivalents of sodium fluoride were used in a 48 hours synthesis, the desired product ï hexagonal sodium yttrium tetrafluoride ï was the only phase detected in XRD (Figure 1). If the synthesis time was shortened to 24 hours, a mixture of the cubic and hexagonal phase was detected, indicating that treatment time is also an important and easily adjustable parameter in performing phase selection.

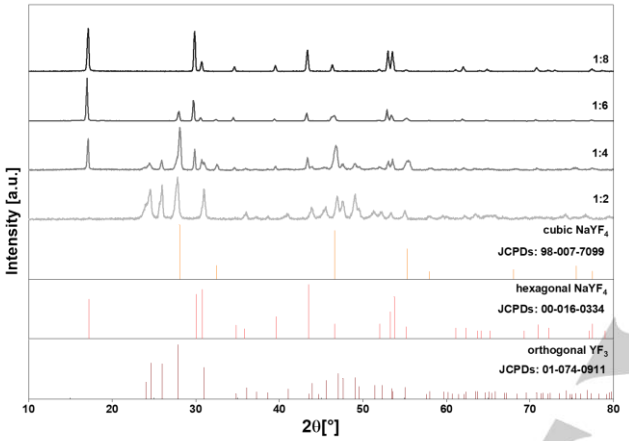

Figure 1. Diffraction patterns of the synthesized products with different Y/NaF ratios (48 hours @ 150 °C) and the reference patterns for YF_3 and cubic and hexagonal $NaYF_4$.

It should be noted that, when comparing the pattern collected from Y014 (see table 10 in the Experimental Section for a full list of the prepared samples) with the reference for hexagonal $NaYF_4$, though the reflection positions agree, the relative intensities show some deviations. In particular, reflections (100) at 17.1°, (110) at 30.1° and (300) at 53.3° appear more intense compared to the reference. The reason for this was hypothesized to be anisotropic growth possibly coupled with texturing effects.

To follow up on this hypothesis, scanning electron microscopy (SEM) measurements were carried out. An exemplary micrograph is presented in Figure 2. The revealed structures were in the range of a few micrometers and displayed an elongated shape, which was both according to expectations and in agreement with XRD outcomes (vide infra). The micrograph features agglomerated rods with an average length of around 6 ε m and a diameter of about 1 ε m. Moreover, it is noticeable that the achieved structures were not homogeneous in size, but rather featured widths between 600 nm and 1.5 µm. This result is not unexpected, as other reports available in literature on the hydrothermal synthesis of $NaYF_4$ document achieving particles measuring several micrometers (e.g. Zhou et al. obtained nanoprisms of a length roughly equal to 6 ε m).[14] To investigate sample dispersability, in view of possible requirements for specific applications, 10 mg of sample Y014 were dispersed in different solvents. It was possible to achieve a stable dispersion in 5 g ethanol, whereas 6 g of solvent were necessary for the same result to be achieved in water and 6.5 g for acetonitrile and in acetone. The suspensions were stable for about twenty minutes. It should be noted that none of these three dispersions showed long-term stability, as they tended to again separate into a liquid phase and a solid deposit within a half hour of the original dispersion. The dispersion in acetone destabilized more quickly than the one in acetonitrile which in turn was less stable than the ones in water and in ethanol (which were roughly equivalent in stability).

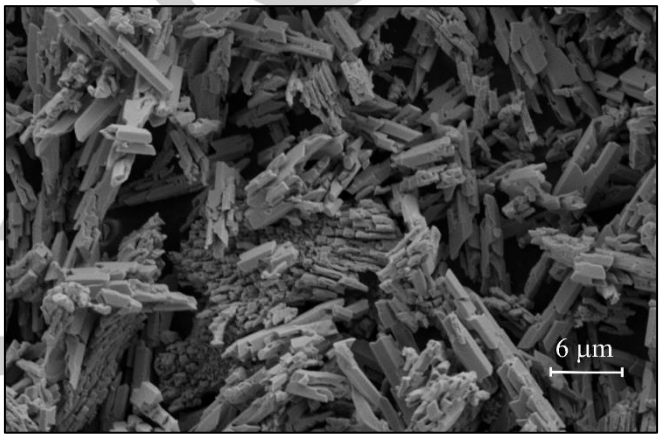

Figure 2. SEM micrograph collected from sample Y014.

To gain more information on the surface, and in particular to evaluate surface composition, chemical environments and possible segregation effects, X-ray photoelectron spectroscopy (XPS) measurements were performed on sample Y014. The corresponding survey spectrum is reported in Figure S1 in Supporting Information.

The XPS survey spectrum included all the expected elements for $NaYF_4$, as well as carbon and oxygen, as adventitious contaminations (which are unavoidable in XPS due to the ubiquitous nature of these two elements in the atmosphere, leading to the formation of a nanolayer featuring carbon and oxygen which is visible to this technique).[15] It should be furthermore noted that the presence of this C and O surface contamination does not imply the presence of such contaminations in the bulk. All peaks could be identified which led to conclude that the sample composition was according to expectations. All binding energies (*BE*s) were corrected for surface charging effects based upon the *BE* value of the measured C1s region (adventitious carbon) compared to literature data (284.6 eV).[16] The Na1s, Y3d and F1s region were further studied through fitting (Figure S2 in Supporting Information). The doublet splitting in the Y3d region (2.0 eV) is in accordance with literature data for YF_3 (2.2 eV).[17] The corrected

10.1002/chem.201903261

FULL PAPER

binding energies for the O1s, Na1s, Y3d, Y3p and F1s regions are reported in Table 1.

Table 1. Corrected binding energies of hexagonal sodium yttrium fluoride sample Y014 compared to literature values[16a] and surface composition in atomic %.

	Na1s	Y3d	Y3p	F1s
BE (sample) [eV]	1071.6	159.5	302.5	685.2
BE (literature) [eV]	1071.4[18]	159.3[18]	299[19]	684.5[18]
quantitative analysis [%][a]	17.2	17.2	-	65.6

[a] C and O were not considered in this computation as they were attributed to surface contamination

The literature value in Table 1 for Y3p is valid for the elemental forms of Yb, which explains why the measured *BE* value is slightly higher compared to the reference. In $NaYF_4$, yttrium is present as an oxidized species with a higher binding energy compared to the pure metal. Moreover, the binding energies are influenced by the chemical environment and neighboring atoms. Disregarding oxygen and carbon, the yttrium atoms are surrounded by fluorine. Fluorine is highly electronegative, which leads to a further increase of the Y3p binding energy.

For the quantitative measurements (see Table 1 above), the 1s peaks were analyzed for sodium and fluorine, whereas for yttrium the 3d region was used. These investigations revealed that the surface Na:Y:F atomic ratio was, as expected, 1:1:4. From that fact it could be assumed that the element distribution was homogeneous throughout the sample surface.

All in all, the characterization suggested that the reaction follows other pathways compared to the proposed one (see Eq. 1 above). The following equations show possible alternative reactions leading to the main crystalline phases visible in the XRD patterns for each sodium fluoride/yttrium nitrate molar ratio:

Y/F = 1:2

□ Eq. 2

Y/F = 1:4

□ Eq. 3

Y/F = 1:8

□ Eq. 4

The bold products are those which could be detected by XRD, whereas the others are soluble in water and were consequently removed during washing. It could be concluded that an excess in sodium fluoride had a positive effect on the reaction, but it was unclear whether it was the excess in sodium or fluorine that was responsible for that.

To better unveil the effect of the nominal amount of sodium employed, the synthesis was repeated for 72 hours at 150 °C, but a part of the sodium fluoride was substituted with sodium nitrate. The product was in all cases a mixture of hexagonal and cubic $NaYF_4$ as well as YF_3 (Figure S3 in Supporting Information). Hence it was concluded that the sodium source has a great influence on reaction and cannot be replaced without other adjustments.

Influence of treatment time

The length of the hydrothermal treatment, during which the heating step takes place (i.e. treatment time), is a parameter that has a significant influence on the synthesis and its outcomes. To identify the optimal treatment time required to yield the desired hexagonal phase, several syntheses were repeated at 150 °C, using yttrium nitrate and sodium fluoride in a 1:8 molar ratio, whilst varying the duration of the hydrothermal treatment from 1 to 48 hours. The corresponding XRD patterns are plotted in Figure 3.

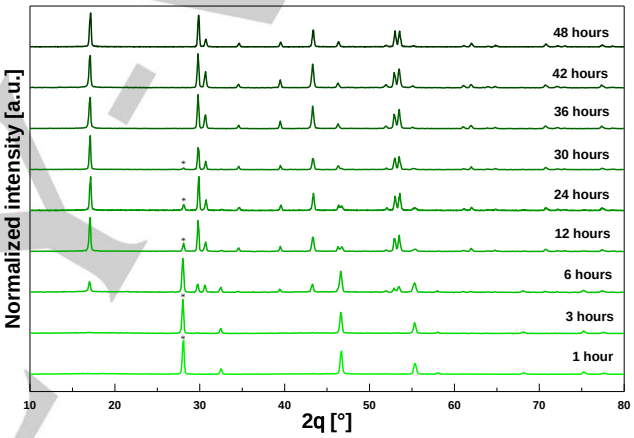

Figure 3. XRD patterns after different treatment times at 150 °C.

The transition from the cubic to the hexagonal phase could broadly be tracked through the diffractograms, by the decreasing intensity of the (111)-reflection, which is the main reflection relative to the cubic phase (at 2 θ = 28.1°, marked with *). After 1 and 3 hours, the whole samples featured only cubic $NaYF_4$ as a crystalline phase. With increasing times, partial transition to the β-phase was observed. Between 6 and 30 hours, a mixture of both phases was detected with the intensity of the reflections relative to the hexagonal $NaYF_4$ becoming more intense with longer reaction times. The reflections ascribable to the cubic phase decrease proportionally. It was concluded that at least 36 hours are necessary for the formation of the pure hexagonal phase.

To more accurately visualize the decreasing amount of cubic $NaYF_4$ compared to the hexagonal phase, Figure 4 shows a plot of the phase composition in terms of weight percentages, as retrieved from the Whole Powder Pattern Fitting (WPPF) procedure carried out using Maud (the results of which are reported in Table 2).

10.1002/chem.201903261

FULL PAPER

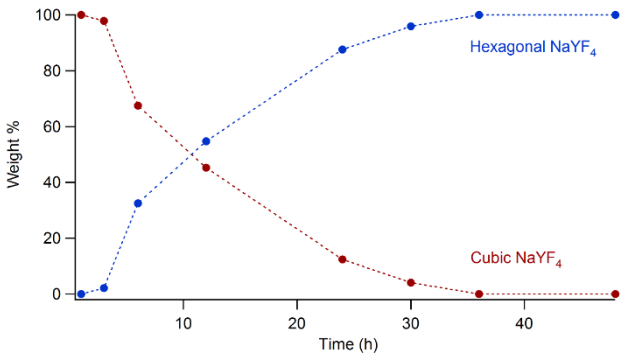

Figure 4. Plot of the phase composition retrieved for samples obtained with different reaction times.

Table 2. Phase composition retrieved for samples obtained with different reaction times.

Sample	Hexagonal $NaYF_4$ (% wt.)	Cubic $NaYF_4$ (% wt.)	Reaction time (h)
Y007	0	100	1
Y008	2	98	3
Y009	33	68	6
Y010	55	45	12
Y011	88	12	24
Y012	96	4	30
Y013	100	0	36
Y014	100	0	48

The figure highlights how only the cubic phase is initially formed and then gradually transitions to the hexagonal one. The transition is completed at 150°C after 36 hours.

Influence of temperature

The last main parameter that was optimized was the synthesis temperature. With the aim of enhancing the sustainability of the synthesis, low temperatures and short reaction times were considered preferable, therefore, synthetic runs were carried out at different temperatures (120 °C, 135 °C and 150 °C) with different treatment times. By observing the bottom half of Figure 5, highlighting the results obtained from syntheses carried out at 135 °C, it appears obvious that the protocol is indeed capable of yielding pure crystalline hexagonal $NaYF_4$, but a greater amount of time (over 72 hours) is required.

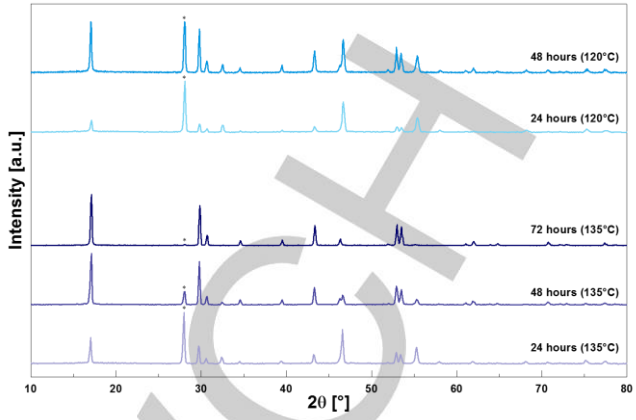

Figure 5. XRD patterns from syntheses carried out at 120 °C for 24, and 48 hours (top) and 135 °C for 24, 48 and 72 hours (bottom).

In all synthesized samples, a mixture of the cubic and hexagonal phase was achieved, recognizable by the (111)-reflection typical of the cubic phase (at 2 ϑ = 28.1°, marked with *). This reflection is still visible after 72 hours (whereas at 150 °C the synthesis reached completion in only half that time - 36 hours). By lowering the temperature to 120 °C, samples yielding the patterns shown in the top section of Figure 5 were obtained, evidencing significant amounts of the cubic phase even after 48 hours.

It can be observed, that compared to samples prepared 135 °C and 150 °C, the time requirement to trigger the transition to the hexagonal phase was further increased. The intensity of the (111)-reflection is relatively high in both samples, leading to the conclusion that the required time to achieve a complete transition to the hexagonal phase is greater than 48 hours. The achieved amount of hexagonal phase (relative to the overall isolated product) is depicted in Figure 6.

As can be seen from the figure, while, for samples treated at 150 °C, the amount of hexagonal $NaYF_4$ was close to 90% after only 24 hours, only 33% and 18% hexagonal phase were obtained for samples treated at 135 °C and 120 °C respectively, showing the significant role of temperature on phase selection.

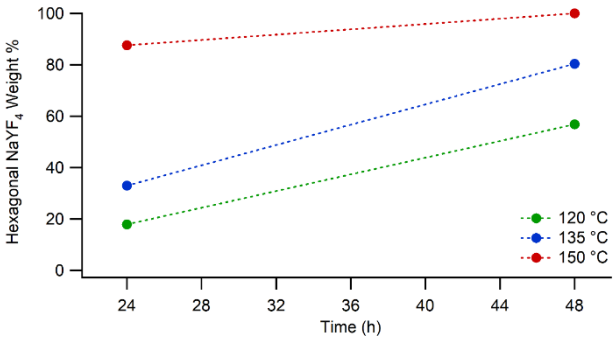

Figure 6. Retrieved amount of hexagonal phase for samples synthetized in 24 h and 48 h at 120 (green), 135 (blue) and 150°C (red).

10.1002/chem.201903261

FULL PAPER

Synthesis of doped sodium yttrium tetrafluoride

Having optimized the synthesis protocol for the host $NaYF_4$ matrix, the accumulated data was applied to the preparation of upconverting doped sodium yttrium tetrafluoride. Regarding this, a part of the yttrium nitrate precursor was replaced by the lanthanide salts, ytterbium and erbium nitrates.

Synthesis of $NaYF_4$ doped with a single-metal

Samples synthetized with a single lanthanoid dopant (Yb or Er) feature the same XRD pattern of the undoped counterpart (Figure 7). Thus, the presence of dopants does not affect the final phase reached after the hydrothermal treatment. Only in two cases ($NaY_{0.96}Er_{0.04}F_4$ and $NaY_{0.94}Er_{0.06}F_4$) the presence of a minor amount of the cubic phase was evident due to the presence of a small reflections at 28.1°, compatible with the (111)-reflection of cubic $NaYF_4$. As it has been documented that, if a $NaYF_4$-structure incorporates late-period lanthanoids (RE ï rare earths), it will show a greater tendency to form a cubic phase $NaREF_4$,[4b] this result is not unexpected. In light of this (also due to the barely perceptible entity of the reflections), it was interpreted as a random imperfection caused by the presence of rare earths.[4b]

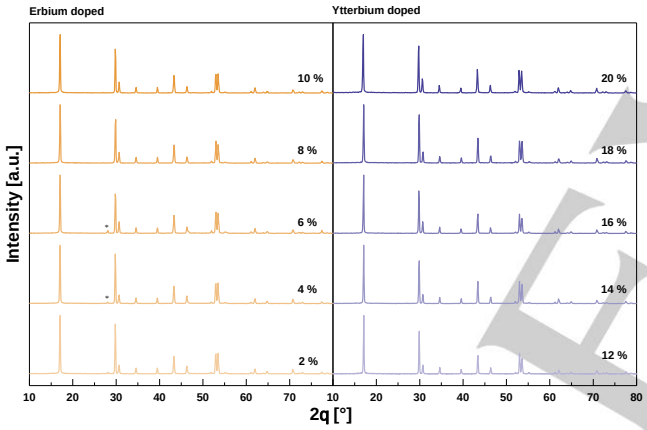

Figure 7. XRD patterns of the erbium and ytterbium doped samples.

While a 72-hour hydrothermal treatment was necessary for the ytterbium doped samples, it was possible to synthesize the erbium doped ones in only 48 hours (both in hexagonal form). To ensure that a pure hexagonal phase is obtained, it was concluded that the longer treatment time (72 hours) is generally preferable when planning a synthesis, as it was seen throughout this work that in many cases a long treatment time was required for a pure hexagonal phase to be yielded.

Generally, dopants can be integrated into a lattice in two different ways, i.e. as interstitial or substitutional dopants. The latter are called antisite defects and can occur if the radii of the host atom and the one of the dopants are similar (within a 14% deviation).[20] As the radii of yttrium, erbium and ytterbium are of the same order of magnitude with a 1-3% size difference,[21] it can be concluded that substitutional doping can take place. Interstitial dopants by contrast occupy vacant sites in the crystal structure, leading to changes in the X-ray diffraction patterns, due to a changed symmetry. The fact that this is not the case further reinforces the conclusion that substitutional doping is occurring.[20a, 22] By refining the cell parameters from the XRD patterns and calculating the relative cell volume, it is evident how the substitution of yttrium with the smaller erbium and ytterbium coherently and proportionally leads to the shrinkage of the unit cell (Figure 8).

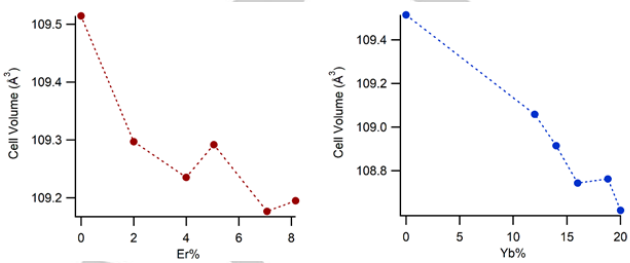

Figure 8. Cell volume calculated for Er-doped (left) and Yb-doped (right) samples against the experimental doping level (form ICP-MS data).

Erbium doping

To verify the actual incorporation of dopants within the synthesized structures, XPS measurements were carried out. Figure S4 in Supporting Information features a comparison between the survey spectra collected from the erbium-doped samples with the lowest and highest amount of erbium versus the spectrum of the pure sodium yttrium fluoride. The doping amount (expressed as **% relative**) is calculated as the molar % ratio between the dopant D and (Y+D) (e.g $NaY_{0.98}Er_{0.02}F_4$ features 2% relative Er doping).

Regardless of the nominal content in the examined samples, no erbium could be detected. Because of this, ICP-MS measurements were necessary to verify the successful doping of the matrix. The results, presented in Table 3, are relative to 2-10 % relative erbium doping.

Table 3. Yttrium and erbium relative content measured by ICP-MS and normalized to Y+Er = 1.

Sample	Nominal composition	Y [%]	Er [%]
Er-Y001	$NaY_{0.98}Er_{0.02}F_4$	98.00	2.00
Er-Y002	$NaY_{0.96}Er_{0.04}F_4$	96.00	4.00
Er-Y003	$NaY_{0.94}Er_{0.06}F_4$	94.95	5.05
Er-Y004	$NaY_{0.92}Er_{0.08}F_4$	92.93	7.07
Er-Y005	$NaY_{0.90}Er_{0.10}F_4$	91.84	8.16

10.1002/chem.201903261

FULL PAPER

Despite the fact that erbium could not be detected by XPS, its actual presence was verified by ICP-MS measurements, verifying that the doping amount could be finely controlled by adjusting the nominal molar ratio between the Er and Y precursors (though the stoichiometry deviated from direct proportionality at higher dopant contents). The highest doping level achieved was 8 % relative, from a nominal doping ratio of 10 % relative (sample Er-Y005).
The fact that erbium was not be detectable through XPS could indicate that erbium tends to segregate inside the material but not on the surface, though it should be noted that trivalent erbium exhibits a strong multiplet splitting[23] leading to a broad signal, which would be difficult to detect at low abundances. Moreover, the expected binding energy is around 168 eV, where the signal would be partly obscured by the overlapping Y3d region.[16a]

Ytterbium doping

The samples with the lowest (12 % relative) and highest (20 % relative) ytterbium doping were investigated by XPS (Figure S5 in Supporting Information). In contrast to the results obtained for erbium, the 4p line could easily be identified in the ytterbium-doped samples.
The survey spectra revealed no obvious changes due to doping, neither in the binding energies or in the relative intensities. The corrected binding energy of the Yb4d peak was measured as 187 eV, which is in agreement with data reported in various publications for trivalent ytterbium species such as YbF_3[17, 23] and in $NaYF_4$.[24] The corrected binding energies of all elements in both samples are collected in Table 4 and are unaltered compared to the undoped sodium yttrium fluoride (see Table 1 above).
Through quantitative analyses of the surface composition a 4:1 Y:Yb atomic ratio was detected in sample Yb-Y001, which is in excellent agreement with the desired composition. For sample Yb-Y005, a 9:1 atomic ratio was measured (as opposed to the expected 7.3:1).

Table 4. Corrected binding energies of the ytterbium-doped $NaYF_4$ samples Yb-Y001 and Yb-Y005 and their surface composition in atomic %.

Sample	Nominal composition		Na1s	Y3d	Yb4d	F1s
Yb-Y001	$NaY_{0.80}Yb_{0.20}F_4$	BE [eV]	1072.1	159.6	187.0	685.4
		quantitative analysis [%]	10	8	2	35
Yb-Y005	$NaY_{0.88}Yb_{0.12}F_4$	BE [eV]	1071.9	159.4	187.1	685.4
		quantitative analysis [%]	17.3	17.3	1.9	63.5

To verify the results achieved by XPS, ICP-MS measurements were additionally performed, and the results are listed in Table 5.

Table 5. Yttrium and ytterbium relative content measured by ICP-MS and normalized to Y+Yb = 1.

Sample	Nominal composition	Y [%]	Yb [%]
Yb-Y001	$NaY_{0.80}Yb_{0.20}F_4$	80.00	20.00
Yb-Y002	$NaY_{0.82}Yb_{0.18}F_4$	81.19	18.81
Yb-Y003	$NaY_{0.84}Yb_{0.16}F_4$	84.00	16.00
Yb-Y004	$NaY_{0.86}Yb_{0.14}F_4$	86.00	14.00
Yb-Y005	$NaY_{0.88}Yb_{0.12}F_4$	88.00	12.00

The ICP-MS measurements results are in agreement with the surface data collected via XPS and reveal that doping was possible with very precise stoichiometric control: only 1% relative deviation was detected in the $NaY_{0.82}Yb_{0.18}F_4$ sample Yb-Y002. The facile hydrothermal synthesis protocol which was optimized is therefore proven to be effective at also affording good control over the product stoichiometry.

Synthesis of co-doped $NaYF_4$

In order to enhance the performance of the functional materials, co-doping was carried out with the same dopant concentrations (in molar % relative to Y+Yb+Er, hereby in **% relative**) as the single lanthanoid doped samples to achieve a better comparability. The overall doping level was 22 % relative in all cases, as only the ratio between ytterbium and erbium was varied. The resulting XRD patterns are shown in Figure 9, all evidencing the same pattern of the undoped sample, thus indicating that the final obtained crystalline structure is still the hexagonal $NaYF_4$.

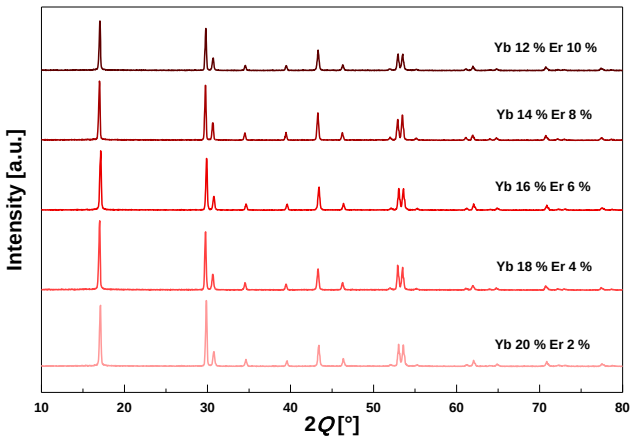

Figure 9. Comparison of the XRD patterns of all co-doped samples.

For the purpose of applying these materials as anti-counterfeit measures in commercial materials, it is important that they i) are

FULL PAPER

non-luminescent in ambient conditions and ii) are luminescent when suitably excited. An additional desirable feature is for the necessary excitation to fall into an energy range where the radiation will not risk causing damage to the examined object (*i.e.* excitation should take place in the NIR, rather than the UV range). In this context, the optical properties of the synthesized materials were investigated by photoluminescence measurements.

The upconversion spectra for the several co-doped samples were measured by exciting at 980 nm with a laser diode and the emission was collected in the visible range, shown in Figure 10. The strongest emission was found for the 20 mol% Yb^{3+} and 2 % Er^{3+} co-doped sample. Emission bands in the visible range can be assigned as follows: $^2H_{11/2} \rightarrow {}^4I_{15/2}$ at 525 nm, $^4S_{3/2} \rightarrow {}^4I_{15/2}$ at 545 nm (green region) and $^4F_{9/2} \rightarrow {}^4I_{15/2}$ at 657 nm (red region), in agreement with similar lanthanide doped fluoride based samples [25], indicating that the exciting radiation energy was upconverted to higher energies in the range of visible light.

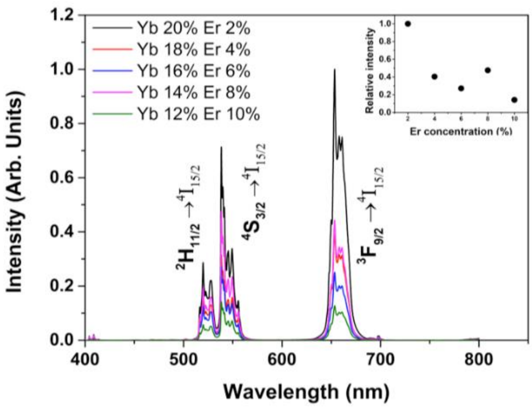

Figure 10. Emission spectra for Er^{3+},Yb^{3+} codoped $NaYF_4$ samples upon 980 nm excitation with a laser diode. Inset: green emission as a function of the Er^{3+} concentration, normalized to the brightest sample.

By comparing the emission of the different samples shown in Figure 10, it can be noted that the luminescence intensity changes significantly with the Er^{3+} concentration. The highest emission intensity is observed for sample Yb/Er-Y001 ($NaY_{0.78}Yb_{0.20}Er_{0.02}F_4$), in agreement with the results found for usual upconverting materials.[8, 26] The luminescence intensity decreases with increasing Er^{3+} concentration in the samples. This behavior can be explained considering that the average distance among the Er^{3+} ions decreases as the concentration increases. Therefore, the cross-relaxation processes present among Er^{3+} ions are more efficient as the average distance between Er^{3+} ions decreases (see inset in Figure 10). To further investigate the upconversion properties and to determine the upconversion order, the Er^{3+} ion emission integrated intensity was measured as a function of the laser excitation power. A log-log plot of the integrated upconversion emission (I_{UC}) versus power density (P_{exc}) of the exciting radiation for the $NaY_{0.78}Yb_{0.2}Er_{0.2}F_4$ is shown in Figure 11. The fits according to the usual relation $I_{UC} \propto P_{exc}^n$ for the upconversion, where *n* is the number of participating photons, are shown in Figure 11, from which it is found that both the excited $^4S_{3/2}$ and $^4F_{9/2}$ levels of the Er^{3+} ions are populated by two photon processes. It is interesting to remark that the upconversion signal for sample Yb/Er-Y001 ($NaY_{0.78}Yb_{0.20}Er_{0.02}F_4$) was observed for laser power densities as low as 0.035 W/cm^2, as shown in the pictures in Figure 11, indicating that the efficiency of the upconversion process for the present material is particularly high.[1b, 27]

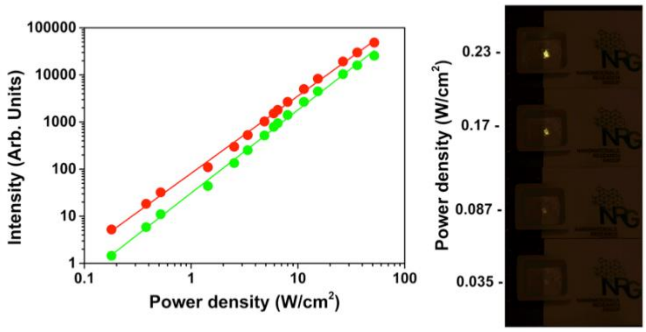

Figure 11. (Left) Excitation power dependence of the green (in the 500-570 nm range) and red (in the 620-700 nm range) emissions under 980 nm laser diode excitation. Green line: power study for the green emission (n=1.76±0.03). Red line: power study for the red emission (n=1.64±0.03). (Right) Pictures of sample Yb/Er-Y001 ($NaY_{0.78}Yb_{0.20}Er_{0.02}F_4$) under different laser excitation power density.

To investigate dopant distribution on the surface, XPS measurements were carried out (Figure S6 in Supporting Information).

As in the single lanthanoid doped samples, no erbium peaks could be observed. In contrast to that, the ytterbium 4d peak could be identified at a corrected binding of 186.3 eV, which is in agreement with the data for trivalent ytterbium as described above.[17, 23-24]

The binding energy of all elements after correction for surface charging and the results of the quantitative analysis are listed in Table 6.

Table 6. Corrected binding energies of Yb/Er-Y001 ($NaY_{0.78}Yb_{0.20}Er_{0.02}F_4$) compared to literature values and atomic percentages from the quantitative analysis.

	Na1s	Y3d	Y3p	Yb4d	Er4d	F1s
BE (sample) [eV]	1071.6	159.0	302.5	186.3	Not detected	685.0
BE (literature) [eV]	1071.4[18]	159.3[18]	299[19]	187[24]	170[19]	684.5[18]
quantitative analysis [%]	16.2	14.7	-	2.9	N/A	66.2

10.1002/chem.201903261

FULL PAPER

As for the single lanthanoid doped samples, no erbium was detected by XPS and for that reason not listed in the above table. The measured values agree with those reported in the literature (relating to trivalent species), though the yttrium and ytterbium peaks display a slight shift to higher binding energies due to their higher oxidation state and chemical surrounding. The quantitative analysis suggests that the doping with ytterbium was successful and yielded samples with the expected composition. Although ytterbium was detected on the sample surface, this does not hold true for erbium (as was the case for all Er-doped samples ï see above). The chemical surface composition, according to XPS, was $NaY_{0.88}Yb_{0.18}F_4$ instead of $NaY_{0.78}Yb_{0.20}Er_{0.02}F_4$. As in the case of the single lanthanoid doped samples, ICP-MS measurements were performed to further investigate the bulk composition. The normalized results are shown in Table 7.

Table 7. Yttrium, ytterbium and erbium relative content measured by ICP-MS and normalized to Y+Er+Yb = 1.

Sample	Nominal composition	Y [%]	Yb [%]	Er [%]
Yb/Er-Y001	$NaY_{0.78}Yb_{0.20}Er_{0.02}F_4$	77.23	20.79	1.98
Yb/Er-Y002	$NaY_{0.78}Yb_{0.18}Er_{0.04}F_4$	77.23	18.81	3.96
Yb/Er-Y003	$NaY_{0.78}Yb_{0.16}Er_{0.06}F_4$	79.59	14.29	6.12
Yb/Er-Y004	$NaY_{0.78}Yb_{0.14}Er_{0.08}F_4$	79.59	15.31	5.10

The obtained results fit the expectation. The highest deviation for erbium was measured in sample Yb/Er-Y004 ($NaY_{0.78}Yb_{0.14}Er_{0.08}F_4$ - 5 % instead of 8 %); by contrast ytterbium displayed the highest deviation in sample Yb/Er-Y003 ($NaY_{0.78}Yb_{0.16}Er_{0.06}F_4$ - by 2 %) and the lowest in sample Yb/Er-Y001 ($NaY_{0.78}Yb_{0.20}Er_{0.02}F_4$).

Conclusions

An easy, green low-temperature route was optimized for the synthesis of upconverting doped $NaYF_4$, allowing to tune, through variations of the experimental parameters, the prevalence and co-occurrence of the two main crystalline phases displayed by the species. Instead of using carcinogen or toxic solvents, the synthesis was performed in water at relatively low temperatures via the hydrothermal approach. Indeed, the effect of temperature, treatment time and precursors on the crystal structure, morphology and composition of the resulting materials was investigated via a plethora of techniques (XRD, XPS, SEM, ICP-MS) and the optimal parameters to yield hexagonal sodium yttrium fluoride were determined. Interestingly, doping with ytterbium and/or erbium were achieved by simple changes in the precursor metals, showing that an excellent degree of control over the final product composition can be reached.
Lanthanide doped sodium yttrium fluoride particles show strong upconversion emission in the green (525 and 545 nm) and in the red region (around 650 nm). The best emitting material was found to be the 20% Yb^{3+} - 2% Er^{3+} doped sample.
The optimized route for the synthesis of the upconverting materials is extremely promising for possible industrial scaling. Possible applications of the present materials range from materials for phosphors to materials for anti-counterfeiting measures, especially in such avenues as shoe wear or fashion. For industrial applications, it might be important to further investigate the possibility of shortening the required thermal treatment, to introduce alternative and less energy demanding thermal treatments (e.g. microwave processing) and to scale-up of the whole process.

Experimental Section

Reagents

Yttrium (III) nitrate hexahydrate (99.8%), erbium (III) nitrate pentahydrate (99.9%), ytterbium (III) nitrate pentahydrate (99.9%) and sodium nitrate (99.5%) were purchased from Merck-Sigma Aldrich (Rodano, Milano). Sodium fluoride (99%) was purchased from Carlo Erba (Cornaredo, Milano). All reagents were used without further treatments or purification.

Synthesis of $NaYF_4$

Hydrothermal synthesis of undoped sodium yttrium fluoride

The first to be addressed was undoped $NaYF_4$, the synthesis of which was carried out by varying several experimental parameters, including the nominal molar ratio of the precursors, the temperature and duration of the hydrothermal treatment. The different molar ratios and reaction conditions are listed in Table 8. For sake of legibility, yttrium nitrate hexahydrate is labelled as $Y(NO_3)_3$.

10.1002/chem.201903261

FULL PAPER

Table 8. Parameters of the hydrothermal synthesis of $NaYF_4$: masses, moles and times of the hydrothermal treatment.

Sample	$Y(NO_3)_3$: NaF	$Y(NO_3)_3$ [mmol]	NaF [mmol]	*t* [h]	*T* [°C]
Y001	1:2	0.50	1.0	24	150
Y002	1:2	0.50	1.0	48	150
Y003	1:4	0.50	2.0	24	150
Y004	1:4	0.50	2.0	48	150
Y005	1:6	0.51	3.00	72	150
Y006	1:7	0.50	3.50	48	150
Y007	1:8	0.51	4.00	1	150
Y008	1:8	0.51	4.00	3	150
Y009	1:8	0.51	4.00	6	150
Y010	1:8	0.51	4.00	12	150
Y011	1:8	0.51	4.00	24	150
Y012	1:8	0.51	4.00	30	150
Y013	1:8	0.51	4.00	36	150
Y014	1:8	0.51	4.00	48	150
Y015	1:8	0.51	4.00	24	135
Y016	1:8	0.51	4.00	48	135
Y017	1:8	0.51	4.00	72	135
Y018	1:8	0.51	4.00	24	120
Y019	1:8	0.51	4.00	48	120
Y020	1:8	0.51	4.00	72	120
Y021	1:8	0.51	4.00	96	120
Y022	1:8	0.51	4.00	120	120

A typical synthesis protocol, carried out with a $Y(NO_3)_3$:NaF = 1:8 molar ratio, is reported below:

Yttrium nitrate hexahydrate (194 mg, 0.51 mmol) and sodium fluoride (168 mg, 4.0 mmol) were dissolved in deionized water (10 mL) under stirring. Then, the solution was hydrothermally treated in a PTFE vessel placed in a stainless steel 4745 General Purpose Acid-Digestion Bomb (Parr Instrument Company) at 150 °C for 24 hours. The resulting particles were isolated by centrifuging for 5 minutes at 10.000 RPM, washed with deionized water and finally dried in air at 80 °C for two hours in an oven. The last two of the three wash cycles were aided by treatment in a sonic bath. A single synthetic run yielded 65 mg (0.36 mmol) of white powdered $NaYF_4$, corresponding to a 72 % yield.

The synthesis was repeated at 135 °C for 24, 48 and 72 hours and at 120 °C for 24, 48 and 72, 96 and 120 hours, with all other parameters kept equal.

Sodium Nitrate as Additional Sodium Source

To explore the influence of sodium fluoride on the synthesis reaction, a portion of this salt was replaced by sodium nitrate as a source of sodium. The corresponding precursor masses and molar ratios are shown in Table 9. The reactants were dissolved in water (10 mL) while stirring. Hydrothermal treatment was performed at 150 °C for 72 hours. The yielded product was washed four times, each as described above and dried at 60 °C.

Table 9. Molar ratios of yttrium nitrate, sodium fluoride and sodium nitrate, as well as the employed molar amounts of substance.

Sample	$Y(NO_3)_3$:NaF:$NaNO_3$	$Y(NO_3)_3$ [mmol]	NaF [mmol]	$NaNO_3$ [mmol]
Y023	1:4:2	0.51	2.0	1.0
Y024	1:3:3	0.51	1.5	1.5
Y025	1:4:4	0.50	2.0	2.0
Y026	1:4:6	0.52	2.0	3.0

Hydrothermal Synthesis of doped sodium yttrium fluoride

The preparation of the lanthanide doped $NaYF_4$ was performed analogously to the undoped samples, except for the substitution of part of the Y^{3+} ions with Yb^{3+} and/or Er^{3+} ones. The experimental details are reported in Table 10, where the nitrates are abbreviated to $Y(NO_3)_3$, $Yb(NO_3)_3$ and $Er(NO_3)_3$.

10.1002/chem.201903261

FULL PAPER

Table 10. Parameters for the synthesis of ytterbium- and erbium-doped sodium yttrium tetrafluoride.

Sample	Composition	$Y(NO_3)_3$ [mmol]	$Yb(NO_3)_3$ [mmol]	$Er(NO_3)_3$ [mmol]
Yb-Y001	$NaY_{0.80}Yb_{0.20}F_4$	0.40	0.10	-
Yb-Y002	$NaY_{0.82}Yb_{0.18}F_4$	0.41	0.09	-
Yb-Y003	$NaY_{0.84}Yb_{0.16}F_4$	0.42	0.08	-
Yb-Y004	$NaY_{0.86}Yb_{0.14}F_4$	0.43	0.07	-
Yb-Y005	$NaY_{0.88}Yb_{0.12}F_4$	0.44	0.06	-
Er-Y001	$NaY_{0.98}Er_{0.02}F_4$	0.49	-	0.01
Er-Y002	$NaY_{0.96}Er_{0.04}F_4$	0.48	-	0.02
Er-Y003	$NaY_{0.94}Er_{0.06}F_4$	0.47	-	0.03
Er-Y004	$NaY_{0.92}Er_{0.08}F_4$	0.46	-	0.04
Er-Y005	$NaY_{0.90}Er_{0.10}F_4$	0.45	-	0.05
Yb/Er-Y001	$NaY_{0.78}Yb_{0.20}Er_{0.02}F_4$	0.40	0.10	0.01
Yb/Er-Y002	$NaY_{0.78}Yb_{0.18}\ Er_{0.04}F_4$	0.39	0.09	0.02
Yb/Er-Y003	$NaY_{0.78}Yb_{0.16}\ Er_{0.06}F_4$	0.39	0.08	0.03
Yb/Er-Y004	$NaY_{0.78}Yb_{0.14}\ Er_{0.08}F_4$	0.38	0.07	0.04
Yb/Er-Y005	$NaY_{0.78}Yb_{0.12}\ Er_{0.10}F_4$	0.39	0.06	0.05

The hydrothermal synthesis was carried out by dissolving all the metal precursors (nitrates) together with sodium fluoride (168 mg, 4.0 mmol) in deionized water (10 mL). The hydrothermal treatment was performed at 150 °C for 72 hours and for 48 hours in case of $NaYF_4:Er^{3+}$. The white powder was washed four times as described above and dried at 60 °C.

Powder X-ray Diffraction

X-ray powder diffraction patterns were collected with a Bruker D8 Advance diffractometer equipped with a Göbel mirror and employing the Cu Kŭ radiation. The angular accuracy was 0.001° and the angular resolution was better than 0.01°. All patterns were recorded in the 10°ï 80° range with a 0.1° (2*θ*) or 0.03°scan step and a 10 s or 7 s per step acquisition time. Obtained patterns were fitted by Whole Powder Pattern Fitting (WPPF) using the software Maud to quantify samples phase compositions and unit cells parameters.[28] Reflections were modeled using asymmetric pseudo-Voigt functions, while background was interpolated using manually selected background points. Samples texture was dealt using an harmonic model.

X-ray Photoelectron Spectroscopy

Powder samples were investigated by XPS with a Perkinï Elmer ű 5600ci instrument using Al Kŭ radiation (1486.6 eV), operating at 350 W. The working pressure was less than $5\cdot10^{ï 8}$ Pa. The calibration was based on the binding energy of the Au $4f_{7/2}$ line at 83.9 eV with respect to the Fermi level. The standard deviation for the *BE* values was 0.15 eV. Reported binding energies were corrected for charging effects, and the binding energy value of 284.6 eV was assigned to the C1s line of carbon.[16] The survey scans were obtained in the 0ï 1350 eV range (pass energy 187.5 eV, 1.0 eV step$^{ï 1}$, 25 ms step$^{ï 1}$) and the detailed scans (29.35 eV pass energy, 0.1 eV step$^{ï 1}$, 50ï 150 ms step$^{ï 1}$) were recorded for O1s, C1s, N1s, F1s, Y3p, Y4p and Yb4p, Er3p and Er4p. The atomic composition was evaluated after a Shirley-type background subtraction.[29] Peak assignment was carried out according to literature data[16a, 16b, 30] and fitting with the KolXPD software.

Luminescence measurements

For the measurement of the upconversion emission, a 980 nm diode laser was used as the radiation source (CNI Optoelectronics Tech). The laser beam was focused on the powder sample and the emission gathered with a 4x objective and a beam splitter (Thorlabs, BSS10), in backscattering mode. The upconversion spectra were recorded using a half-meter monochromator (Andor, Shamrock 500i) equipped with a 300 lines mm^{-1} grating and CCD detector (Andor, iDus420-BVF). The digital pictures were obtained with a Canon eos 600d camera.

Scanning Electron Microscopy

Measurements were performed by using a Field Emission (FE-SEM) Zeiss SUPRA 40VP, with a primary beam acceleration voltage of 5 kV and a conventional secondary electron detector.

Inductively Coupled Plasma-Mass Spectrometry

Chemicals and Procedure: Samples were measured by using an Agilent Technologies 7700x ICP-MS system (Agilent Technologies International Japan, Ltd., Tokyo, Japan), equipped with an octopole collision cell and operated in kinetic-energy discrimination mode, utilized for the removal of polyatomic interferences and argon-based interferences. The instruments were optimized daily to achieve optimum sensitivity and stability, according to manufacturer recommendations. Y, Yb, Er (all 10 mg L$^{ï 1}$) were present in the ICP-MS multielement calibration standard-1 (no. 8500-6944, Agilent Technology). All solutions were prepared in milliQ Ultrapure water, obtained with a Millipore Plus System (Milan, Italy, resistivity 18.2 Mohm cm$^{ï 1}$). ICP-MS system was tuned daily using a tuning solution (1 εg L$^{ï 1}$, no. 5184-3566, Agilent Technologies, UK) containing ^{140}Ce, ^{7}Li, ^{205}Tl, and ^{89}Y. An internal standard solution (100 εg L$^{ï 1}$, no. 5183-4681, Agilent Technology) of ^{45}Sc and ^{115}In, prepared in nitric acid [3 % (w/w)] was used as the internal standard by addition to the sample solution through a T-junction.

Sample Digestion: 10-15 mg of the samples were dissolved in 3.5 g HNO_3 (69 % w/w) and heated to 100°C in a water bath for half an hour. The vials were then cooled, and the obtained solutions were diluted with 51.5 g water. 0.30 g of the solution were diluted in 14.7 g HNO_3 [3 % (w/w)].

Keywords: hydrothermal synthesis Ådoping Åupconversion Å low-temperature Åfluoride

[1] a) J. Zhou, Q. Liu, W. Feng, Y. Sun, F. Li, *Chem. Rev.* **2015**, 115, 395; b) S. Wen, J. Zhou, K. Zheng, A. Bednarkiewicz, X. Liu, D. Jin, *Nat. Commun.* **2018**, 9, 2415; c) L. Sun, R. Wei, J. Feng, H. Zhang, *Coord. Chem. Rev.* **2018**, 364, 10.

[2] a) H. H. Gorris, O. S. Wolfbeis, *Angew. Chem. Int. Edit.* **2013**, 52, 3584; b) H. H. Gorris, O. S. Wolfbeis, *Angew. Chem.* **2013**, 125, 3668; c) J. Liu, H. Rijckaert, M. Zeng, K. Haustraete, B. Laforce, L. Vincze, I. Van Driessche, A. M. Kaczmarek, R. Van Deun, *Adv. Funct. Mater.* **2018**, 28, 1707365.

[3] a) W. Yao, Q. Tian, J. Liu, Q. Xue, M. Li, L. Liu, Q. Lu, W. Wu, *Nanoscale* **2017**, 9, 15982; b) L. Wang, Y. Li, *Chem. Mater.* **2007**, 19, 727; c) M.-K. Tsang, G. Bai, J. Hao, *Chem. Soc. Rev.* **2015**, 44, 1585; d) M. You, J. Zhong, Y. Hong, Z. Duan, M. Lin, F. Xu, *Nanoscale* **2015**, 7, 4423.

[4] a) J. Wang, H. Song, W. Xu, B. Dong, S. Xu, B. Chen, W. Yu, S. Zhang, *Nanoscale* **2013**, 5, 3412; b) F. Wang, Y. Han, C. S. Lim, Y. Lu, J. Wang, J. Xu, H. Chen, C. Zhang, M. Hong, X. Liu, *Nature* **2010**, 463, 1061.

[5] B. Huang, H. Dong, K.-L. Wong, L.-D. Sun, C.-H. Yan, *J. Phys. Chem. C* **2016**, 120, 18858.

[6] a) M.-A. Einarsrud, T. Grande, *Chem. Soc. Rev.* **2014**, 43, 2187; b) S. Diodati, P. Dolcet, M. Casarin, S. Gross, *Chem. Rev.* **2015**, 115, 11449.

[7] a) B. L. Cushing, V. L. Kolesnichenko, C. J. O'Connor, *Chem. Rev.* **2004**, 104, 3893; b) S. Diodati, L. Pandolfo, S. Gialanella, A. Caneschi, S. Gross, *Nano Res.* **2014**, 7, 1027.

[8] Y. Ma, M. Chen, M. Li, *Mater. Lett.* **2015**, 139, 22.

[9] Y. Wang, R. Cai, Z. Liu, *CrystEngComm* **2011**, 13, 1772.

[10] a) L. Yang, Z. Wang, T. Zhao, Y. Zhong, Y. Liu, *Mater. Express* **2018**, 8, 199; b) M. Ding, J. Hou, Z. Cui, H. Gao, C. Lu, J. Xi, Z. Ji, D. Chen, *Ceram. Int.* **2018**, 44, 7930; c) C. Li, Z. Quan, J. Yang, P. Yang, J. Lin, *Inorg. Chem.* **2007**, 46, 6329; d) C. Li, J. Yang, Z. Quan, P. Yang, D. Kong, J. Lin, *Chem. Mater.* **2007**, 19, 4933.

[11] a) J.-C. Boyer, L. A. Cuccia, J. A. Capobianco, *Nano Lett.* **2007**, 7, 847; b) M. R. Catalano, A. L. Pellegrino, P. Rossi, P. Paoli, P. Cortelletti, M. Pedroni, A. Speghini, G. Malandrino, *New J. Chem.* **2017**, 41, 4771; c) G. Dal Cortivo, G. E. Wagner, P. Cortelletti, K. M. Padmanabha Das, K. Zangger, A. Speghini, D. Dell'Orco, N. H. Meyer, *Sci. Rep.* **2018**, 8, 3420.

[12] P. T. Anastas, J. C. Warner, *Green Chemistry Theory and Practice, Paperback Ed.*, Oxford University Press, New York **2000**.

[13] R. E. Thoma, G. M. Hebert, H. Insley, C. F. Weaver, *Inorganic Chemistry* **1963**, 2, 1005.

[14] S. Zhou, K. Deng, X. Wei, G. Jiang, C. Duan, Y. Chen, M. Yin, *Opt. Commun.* **2013**, 291, 138.

[15] a) S. Evans, *Surf. Interface Anal.* **1997**, 25, 924; b) C. E. Taylor, S. D. Garvey, J. E. Pemberton, *Anal. Chem.* **1996**, 68, 2401.

[16] a) J. F. Moulder, W. F. Stickle, P. E. Sobol, K. D. Bomben, *Handbook of X-Ray Photoelectron Spectroscopy - A Reference Book of Standard Spectra for Identification and Interpretation of XPS Data*, Perkin-Elmer Corp., Eden Prarie, Minnesota **1992**; b) D. Briggs, M. P. Seah, *Practical Surface Analysis - Volume 1 - Auger and X-ray Photoelectron Spectroscopy, 2nd Ed.*, John Wiley & Sons, New York **1990**; c) Z. G. Wang, X. T. Zu, S. Zhu, L. M. Wang, *Phys. E.* **2006**, 35, 199.

[17] Y. Uwamino, A. Tsuge, T. Ishizuka, H. Yamatera, *Bull. Chem. Soc. Jpn.* **1986**, 59, 2263.

[18] M. Tou, Z. Luo, S. Bai, F. Liu, Q. Chai, S. Li, Z. Li, *Mat. Sci. Eng. C* **2017**, 70, 1141.

[19] *NIST XPS Database - Version 3.5; http://srdata.nist.gov/xps/*.

[20] a) S. Hunklinger, *Festkörperphysik*, De Gruyter, Berlin **2018**; b) T. Gerthsen, *Chemie für den Maschinenbau*, Universitätsverlag, Karlsruhe **2006**.

[21] A. F. Holleman, E. Wieberg, *Lehrbuch der Anorganischen Chemie, 101th Ed.*, Walter de Gruyter, New York **1995**.

[22] U. Rössler, *Solid State Theory: An Introduction*, Springer, Berlin **2009**.

[23] H. Ogasawara, A. Kotani, B. T. Thole, *Phys. Rev. B* **1994**, 50, 12332.

[24] Q. Tian, K. Tao, K. Sun, in *Micro Nano Lett.*, Vol. 8, Institution of Engineering and Technology, 2013, 731.

[25] a) M. Pedroni, F. Piccinelli, T. Passuello, M. Giarola, G. Mariotto, S. Polizzi, M. Bettinelli, A. Speghini, *Nanoscale* **2011**, 3, 1456; b) E. W. Barrera, Q. Madueño, F. J. Novegil, A. Speghini, M. Bettinelli, *Opt. Mater.* **2018**, 84, 354.

[26] a) S.-N. Shan, X.-Y. Wang, N.-Q. Jia, *Nanoscale Res. Lett.* **2011**, 6, 539; b) Y. Pu, L. Lin, D. Wang, J.-X. Wang, J. Qian, J.-F. Chen, *J. Colloid Interf. Sci.* **2018**, 511, 243.

[27] M. Kaiser, C. Würth, M. Kraft, I. Hyppänen, T. Soukka, U. Resch-Genger, *Nanoscale* **2017**, 9, 10051.

[28] L. Lutterotti, *Nucl. Instruments Methods Phys. Res. Sect. B Beam Interact. with Mater. Atoms* **2010**, 268, 334.

[29] J. E. Castle, A. M. Salvi, *J. Vac. Sci. Technol., A* **2001**, 19, 1170.

[30] D. Briggs, *Handbook of X-Ray and Ultraviolet Photoelectron Spectroscopy, 1st Ed.*, Heyden & Son Ltd., London **1978**.

10.1002/chem.201903261

FULL PAPER

Entry for the Table of Contents (Please choose one layout)

Layout 1:

FULL PAPER

An effective easy, low-temperature green route was employed for the hydrothermal synthesis of upconverting doped sodium yttrium fluoride ($NaYF_4$:Yb, Er). The materials were then thoroughly characterized through complementary analytical methods from a structural (XRD), morphological (SEM, TEM) and compositional (ICP-MS, XPS) point of view. Photoluminescence measurements were employed to investigate the material's response under NIR irradiation showing upconversion to the red and green visible light regions.

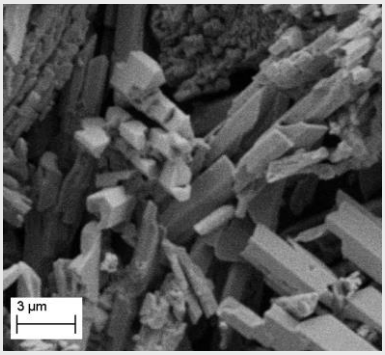

*Nora Jannsen, Stefano Diodati, Nicola Dengo, Francesca Tajoli, Nicola Vicentini, Giacomo Lucchini, Adolfo Speghini, Denis Badocco, Paolo Pastore and Silvia Gross**

Page No. – Page No.

Exploring the Phase-Selective, Green Hydrothermal Synthesis of Upconverting Doped Sodium Yttrium Fluoride: Effects of Temperature, Time and Precursors